Article ID: 1006-8775(2019) 03-0312-12

NUMERICAL PREDICTION OF AN EXTREME RAINSTORM OVER THE PEARL RIVER DELTA REGION ON 7 MAY 2017 BASED ON WRF–ENKF

XIAO Hui (肖 辉)[1], WAN Qi-lin (万齐林)[1], LIU Xian-tong (刘显通)[1], ZHENG Teng-fei (郑腾飞)[1], FENG Lu (冯 璐)[1], XIA Feng (夏 丰)[1], CHEN Jing-hua (陈景华)[2]

(1. Guangzhou Institute of Tropical and Marine Meteorology, CMA, Guangzhou 510641 China; 2. Nanjing University of Information Science and Technology, Nanjing 210044 China)

Abstract: An ensemble Kalman filter based on the Weather Research and Forecasting Model (WRF-EnKF) is used to explore the effectiveness of the assimilation of surface observation data in an extreme local rainstorm over the Pearl River Delta region on 7 May 2017. Before the occurrence of rainstorm, the signals of weather forecasts in this case are too weak to be predicted by numerical weather model, but the surface temperature over the urban area are high. The results of this study show that the wind field, temperature, and water vapor are obviously adjusted by assimilating surface data of 10-m wind, 2-m temperature, and 2-m water vapor mixing ratio at 2300 BST 6 May, especially below the height of 2 km. The southerly wind over the Pearl River Delta region is enhanced, and the convergence of wind over the northern Guangzhou city is also enhanced. Additionally, temperature, water vapor mixing ratio and pseudoequivalent potential temperature are obviously increased over the urban region, providing favorable conditions for the occurrence of heavy precipitation. After assimilation, the predictions of 12-h rainfall amount, temperature, and relative humidity are significantly improved, and the rainfall intensity and distribution in this case can be successfully reproduced. Moreover, sensitivity tests suggest that the assimilation of 2-m temperature is the key to predict this extreme rainfall and just assimilating data of surface wind or water vapor is not workable, implying that urban heat island effect may be an important factor in this extreme rainstorm.

Key words: extreme rainfall; 2-m temperature; assimilation of surface observations; WRF-EnKF; rainstorm

CLC number: P435 **Document code:** A

doi: 10.16555/j.1006-8775.2019.03.003

1 INTRODUCTION

Guangdong Province locates in the south of China. Being an important economic center of China, it is also one of the provinces that suffer the most severe meteorological disasters. Frequent occurrences of the extremely heavy rainfall and severe convective weather events have caused major property losses in this region. Compared to other regions, there are more advantaged conditions of moisture and heat supplied to intense rainfall in southern China. Rainstorm in southern China is one of the hot spots of current research, especially the pre-summer rainy season precipitation (April-June), with the characteristics of complex environment conditions and triggering mechanism, strong suddenness, and strong localization (Zhang et al. [1]; Luo et al. [2]). These complex factors pose a major challenge to numerical weather prediction (NWP) for southern China. Moreover, the study on the physical mechanism of rainstorm is neither systematic nor deep enough (Luo et al. [2]), leading to limited capacity of numerical weather prediction for rainstorm. At present, data assimilation is one of the important means of improving numerical forecast capacity and will allow researchers to probe the development mechanism of disastrous weather systems.

In recent years, the prediction of heavy rainfall in southern China has been studied widely. Based on the works of Zhang et al.[3] and Weng and Zhang [4], Zhu et al. [5] explored the performance of WRF-EnKF in continuous assimilation of Doppler radar data during the landfall of Tropical Cyclone (TC) Vicente (2012). The result showed that assimilating ground-based radar radial velocity could improve the description of TC inner-core structure and the forecasts of the TC track and the associated heavy precipitation inland. In addition, Bao et al. [6] investigated the performance of WRF-EnKF in assimilating radar radial velocity data for the prediction of mesoscale convective systems (MCSs) over southern China during the pre-summer rainy season and showed that the experiment with shortest assimilated time interval and maximum assimilated window tends to give the best performance. Based on radar data in the southern China region, Zhang et al. [7] showed that assimilating

Received 2018-01-09; **Revised** 2019-05-06; **Accepted** 2019-08-15

Foundation item: National Key Basic Research and Development (973) Program of China (2015CB452802); National Natural Science Foundation of China (41705120, 41705020, 41705118); National Science and Technology Program (2017YFC1501701); Guangdong Province Science and Technology Project (2015B020217001, 2017B020244002)

Biography: XIAO Hui, Ph. D., Research Assistant, primarily undertaking research on physics of cloud and precipitation.

Corresponding author: WAN Qi-lin, e-mail: qlwan@gd121.cn

radar-retrieved water vapor could improve the accuracy of short-range precipitation prediction (~12h) under warm start situation.

In the application of other data, Wan and Xu [8] used WRF and the Gridpoint Statistical Interpolation (GSI) data assimilation to employ the Advanced (TIROS) -N [Television and Infrared Observation Satellite] Operational Vertical Sounder (ATOVS) radiance observations and to investigate the evolution and structure of rainstorms associated with a flash-flood event that occurred in central Guangdong. They suggested that the assimilation of radiance data produced better short-range precipitation forecast and the improvement was mainly limited to the forecast range of about 20 hours (Wan et al.[9]). Because the observations from radar and satellite aren't directly used for assimilation, the efficiency of assimilation in NWP model is uncertain to some extent. Moreover, there still exist many problems in the retrieval results from radar and satellite.

Besides the application of radar and satellite data, surface station observation is one of important rainstorm inspection methods. Surface observation has many merits, such as high density, wide distribution, and assimilation without data retrieval. The assimilation of surface observation can influence the vertical structure of the boundary layer during the day (Hacker and Snyder [10]), and can reduce prediction error of storms (Zhang et al. [11]). Huang et al.[12] showed that assimilating surface pressure leads to better forecasting of sea level pressure and precipitation in southern China, especially the forecast of moderate and heavy rain.

Along with economic development, the survival environment of human is changing continually, and urbanization seriously affects the environment and local atmospheric conditions. The change of surface condition and more heat produced by human activity lead to higher temperature in city compared to surrounding areas. This phenomenon is known as urban heat island (Oke [13]; Magee et al.[14]). Huff and Changnon [15] suggested that urban heat island can lead to more instability in atmosphere and more precipitation in the downwind of some cities. In southern China, the Pearl River Delta region with rapid economic growth becomes increasingly urbanized and there is enough water vapor from the South China Sea. In such situations, accurate description of urban heat island effect may play a vital role in precipitation prediction, especially the prediction of extreme local precipitation.

Previous studies are mainly concentrated in the prediction of typhoon and mesoscale convective systems, but the research of extremely heavy rainfall in southern China is rather little, especially the prediction of extremely heavy rainfall in the Pearl River Delta region. In NWP, variational assimilation and EnKF are the most characteristic methods. Compared with variation method, EnKF method has a big computational workload and it can provide a flow-dependent background error covariance (Evensen [16]; Houtekamer et al.[17]; Zhang et al.[18]). Hence, the WRF-EnKF is used to investigate the heavy rainfall process in Guangzhou city (the center of the Pearl River Delta region) on May 7, 2017. The purpose of this work is twofold: 1) to examine the prediction and predictability of local extremely heavy rainfall in southern China based on the WRF-EnKF system; 2) to investigate the significance of urban heat island effect in this process.

2 CASE OVERVIEW

This study investigates the extremely heavy rainfall that occurred in the Pearl River Delta region on May 7, 2017. From the early morning of May 7, there was a large amount of rainfall in northern Guangzhou and it had the following characteristics: highly local, slowness of movement, and great intensity. Fig. 1 shows the major features of synoptic background about this extreme rainfall event. At 2000 Beijing Standard Time (BST), the Pearl River Delta region is dominated by westerly wind under the influence of the subtropical high pressure at 500 hPa, and the region is dominated by southerly wind without obvious convergence at 850 hPa. In addition, the 2-m temperature at 2300 BST (before this process) is also shown in Fig. 1. Compared with the temperature of other regions, the temperature of the Pearl River Delta region appears to be on the high side, especially those of Guangzhou city and Foshan city, which are with obvious thermal island effect.

Figure 2 shows the combined reflectivity of Guangzhou radar during the process. At 2300 BST, there is no obvious radar echoes over the Pearl River Delta region. About 0100 BST (May 7), obvious radar echo has been observed over Huadu District (Guangzhou), and it is enhanced within an hour (Fig. 2b). The precipitation first emerged in Huadu District, and it then expanded its range southward with slow movement and long enduring time (Fig. 2c), setting new records in Guangzhou daily rainfall and 3-hours rainfall of Guangdong province. Maximum 1-hour rainfall amount of over 100 mm appeared in Huadu District, Zengcheng District, and Huangpu District of Guangzhou. Among of them, there is 184.4 mm of rain within one hour in Xintang station (Zengcheng District, Guangzhou). There are five stations over 250mm within one day and the 24-hours cumulative precipitation of Xintangzhen in Zengcheng District is 401.6mm. In general, heavy precipitation is most commonly triggered by frontal systems, shear line, low level jets, and west wind trough, but the signals of these systems are too weak in this case, leading to a difficult prediction from numerical weather prediction model. Hence, what is the key factor to trigger this precipitation and to predict the heavy precipitation?

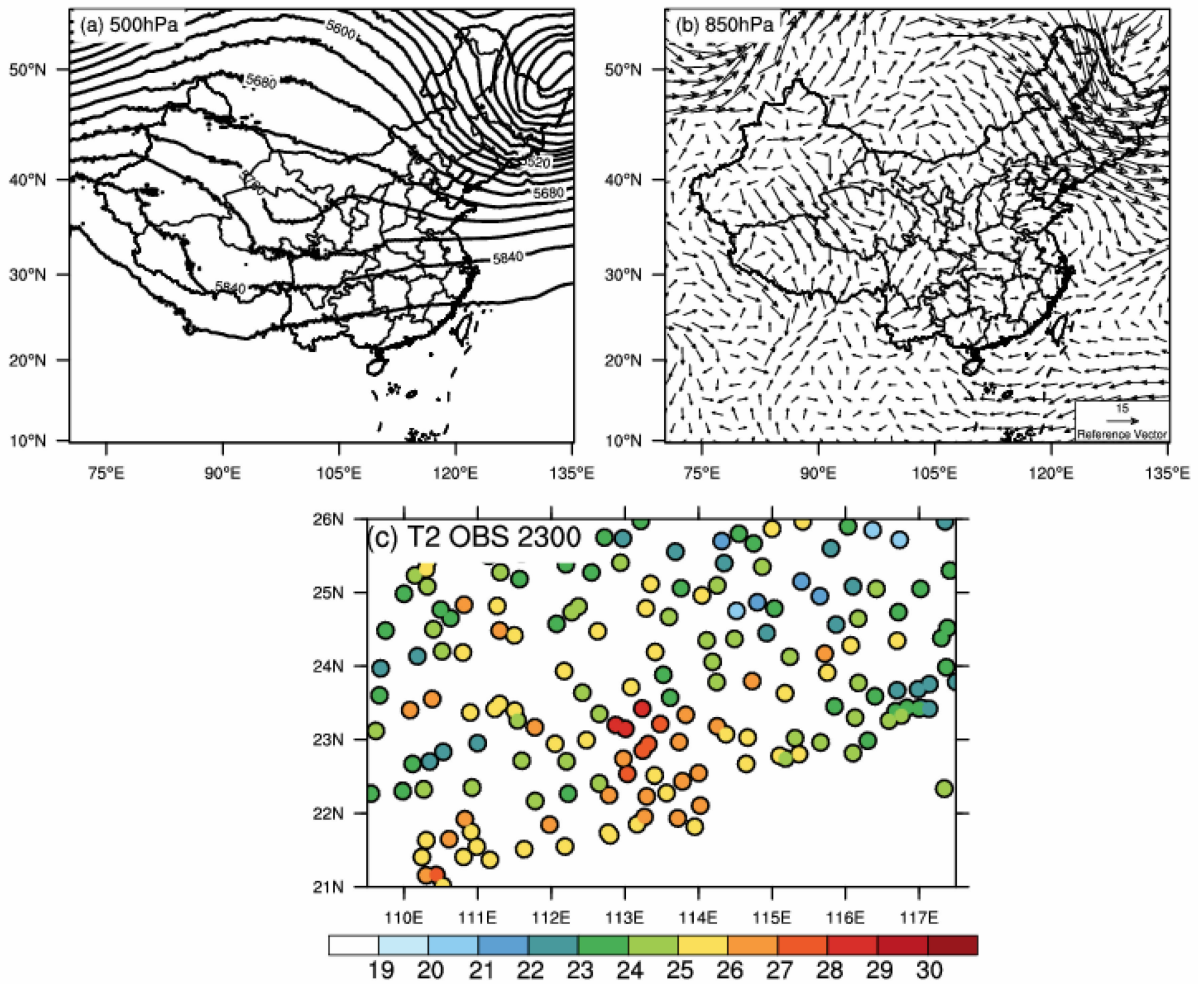

Figure 1. (a) NCEP reanalysis for 500 hPa geopotential height field (gpm), (b) 850 hPa wind field (m/s) at 2000 BST, and (c) surface observation of 2-m temperature (℃) at 2300 BST, 6 May 2017.

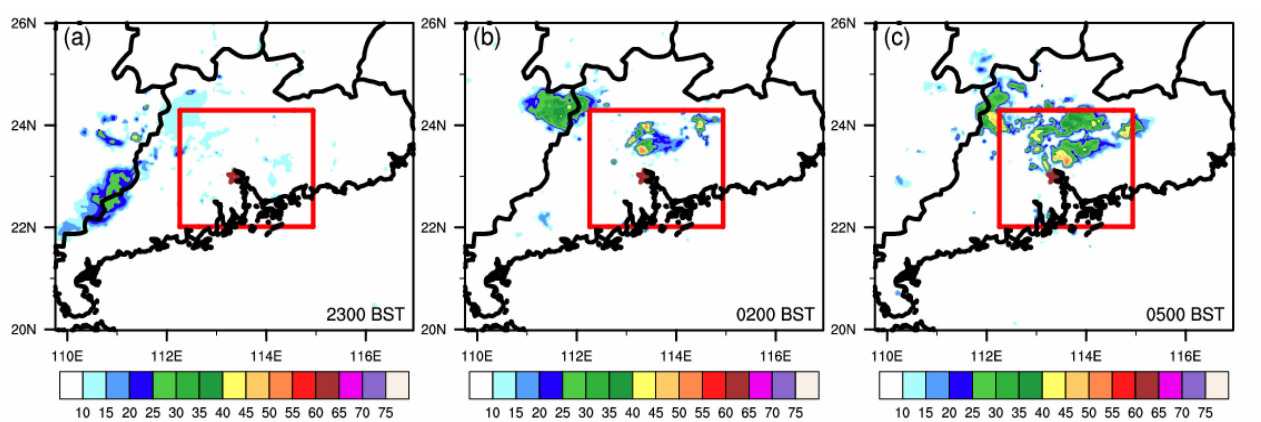

Figure 2. Radar combined reflectivity (dBZ) derived from the Guangzhou radar (red star) during the process: (a)2300 BST 6 May, (b) 0200 BST 7 May, and (c)0500 BST 7 May.

3 DESIGN OF MODEL AND EXPERIMENT

The Weather Research and Forecasting model with ensemble Kalman filter (WRF-EnKF) is used in this study. EnKF, which is internationally recognized as one of the most advanced methods for NWP, can provide a flow-dependent background error covariance. The WRF-EnKF system used in this study is the same as that in Meng and Zhang [19, 20], Zhang et al. [3], and Weng and Zhang [4], which is originally developed for regional-scale data assimilation at the Pennsylvania State University. Three two-way nested domains are conducted with 35 levels in the vertical direction (eta=1.0, 0.99258, 0.98275, 0.96996, 0.95372, 0.93357, 0.90913, 0.87957, 0.84531,

0.80683, 0.76467, 0.7194, 0.67163, 0.62198, 0.57108, 0.51956, 0.46803, 0.4203, 0.37613, 0.33532, 0.29764, 0.2629, 0.23092, 0.20152, 0.17452, 0.14978, 0.12714, 0.10646, 0.08761, 0.07045, 0.05466, 0.03981, 0.0258, 0.01258, and 0.0000). The grid points of domains are 230×165, 381×291, and 541×501 in the horizontal with grid spacings of 12.5, 2.5, and 0.5 km, respectively (Fig. 3). The Morrison double-moment microphysics scheme (Morrison and Pinto [21]), the YSU planetary boundary layer scheme (Noh et al. [22]), and the Grell-Freitas ensemble cumulus scheme (Grell and Freitas [23]; only for domain 1) are also used for this work.

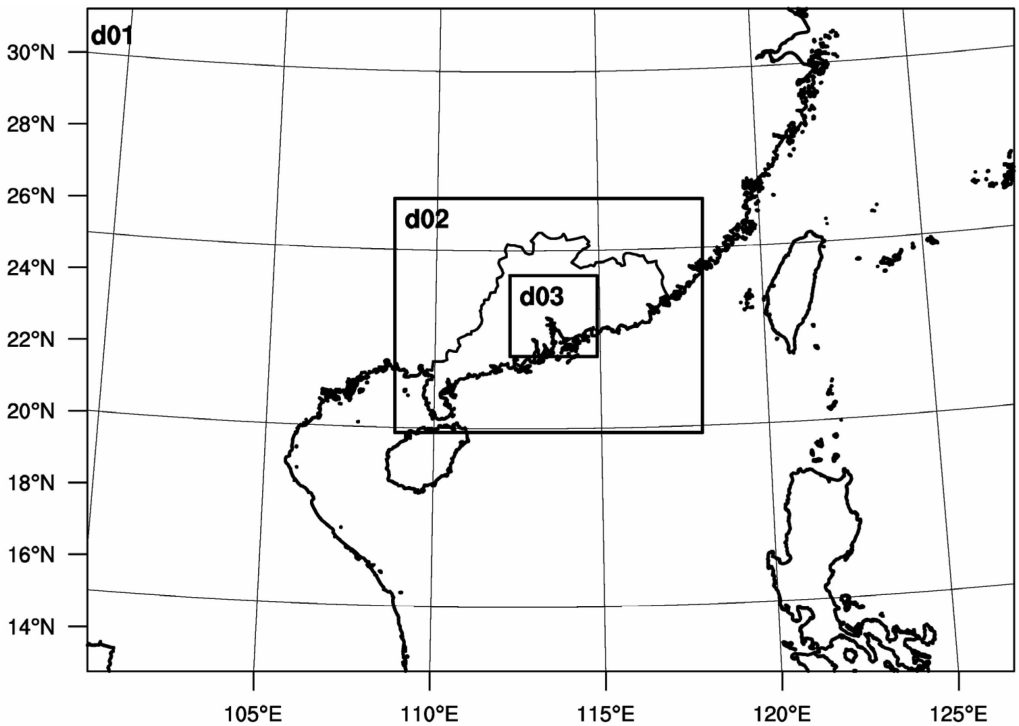

Figure 3. Model domain configuration.

According to the settings of Zhang et al.[3] and Zhu et al.[5], the ensemble number is 60 and the initial ensemble members are produced by adding perturbations to the National Centers for Environmental Prediction/Global Forecast System (NCEP/GFS) data at 2000 BST 6 May 2017. The perturbations are randomly sampled from the default "cv3" background error covariance option in the WRF 3DVar package. The perturbed variables include horizontal (u- and v-) wind components, potential temperature and water vapor mixing ratio (the standard deviations are 2 m/s for wind, 1 K for temperature, and 0.5 g/kg for mixing ratio of water vapor) (Li et al. [24]). Additionally, similar method of perturbations is used for the lateral boundary. The covariance relaxation method is used to inflate the background error covariance with a relaxation coefficient of 0.8. The value of the localization radius is 30 km for observation data. See Zhu et al.[5] for more information.

The 0.25°×0.25° NCEP/GFS (http://www.nco.ncep.noaa.gov/pmb/products/gfs/) is used for the initial and boundary conditions of the system. The surface observation data of Guangdong and neighboring Guangxi, Hunan, Jiangxi, Fujian, and Hainan, includes 2-m temperature, 2-m dew point temperature, rainfall amount, and 10-m wind of national station (Fig. 4). The data of 2-m temperature and 2-m dew point temperature are used to calculate mixing ratio of vapor for subsequent assimilation. From above description, the near-surface temperature of the Pearl River Delta region is higher than other regions and the urban heat island effect is obvious. Moreover, hours before the extreme rainfall event, there is not obviously signal from radar. Hence, the usage of surface observation data is of importance to the prediction of this process.

Figure 5 shows the schematic flowchart for our experiments. The 60 ensemble numbers are first integrated for 3 h (from 2000 BST to 2300 BST 6 May 2017) to develop a high-resolution flow-dependent background error covariance structure. At 2300 BST, the observation data of 10-m wind, 2-m temperature, and 2-m water vapor mixing ratio are assimilated in the innermost domain, and then deterministic forecasts are initiated from the ensemble mean of the EnKF analyses. In this work, experiment "NoDA" is performed as a deterministic forecast initiated from the ensemble mean of the EnKF system without assimilating observation, while experiment "WithDA" with data assimilation. Both experiments are integrated from 2300 BST 6 May to 1100 BST 7 May (12-h forecast).

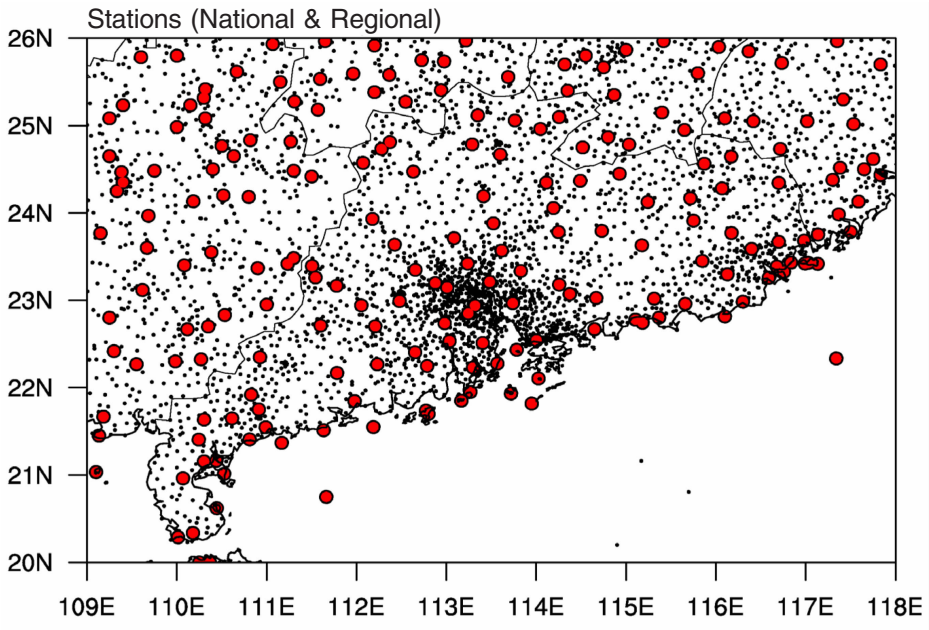

Figure 4. The surface observation stations (red: national station).

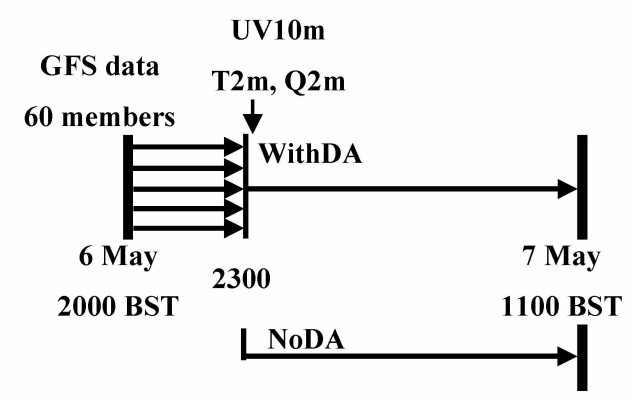

Figure 5. The schematic flowchart of experiments (NoDA: without assimilation; WithDA: with assimilation).

4 SIGLE POINT TEST OF ASSIMILATION

To advance the understanding of the flow-dependent characteristic of EnKF system, assimilation of a single station data is conducted at 2300 BST for system testing. In domain 3, the changes of model variables and their spatial distribution are investigated after assimilating a single station data of 2-m temperature (T=302.35K; longitude=113.231° E; latitude=23.132° N), while the 2m temperature is 297.81K before assimilation. Fig. 6 shows the horizontal distributions of the increments of 2-m temperature and 10-m wind field after assimilating at 2300 BST. In general, the distribution of the increment of 2-m temperature is characterized by a roughly circular with asymmetrical and heterogeneous feature around the observation station, and it is not entirely circular. After assimilation of data, the 2-m temperature within about 30 km radius around the station is increased, and the 2-m water vapor mixing ratio, 10-m wind, and surface skin temperature change correspondingly (not shown). Moreover, the horizontal distributions of them also display asymmetrical feature. The 2-m mixing ratio of water vapor and surface skin temperature increases around the observation station (not shown) and the southerly wind near the surface is enhanced after assimilation of single point data.

Figure 7 shows the vertical increments of temperature, water vapor, and wind along the station (longitude=113.231° E) after assimilating single point data. In vertical direction, the temperature below the height of 2 km is increased after assimilation, especially below the height of 300 m. Additionally, the increasing amplitude of temperature slows down with height. Similar to the change of temperature above, the southerly wind is enhanced, and water vapor is increased in the surface layer. In other words, enhanced southerly wind brings more water vapor to observation station from neighboring sea (the South China Sea), resulting in higher mixing ratio of water vapor.

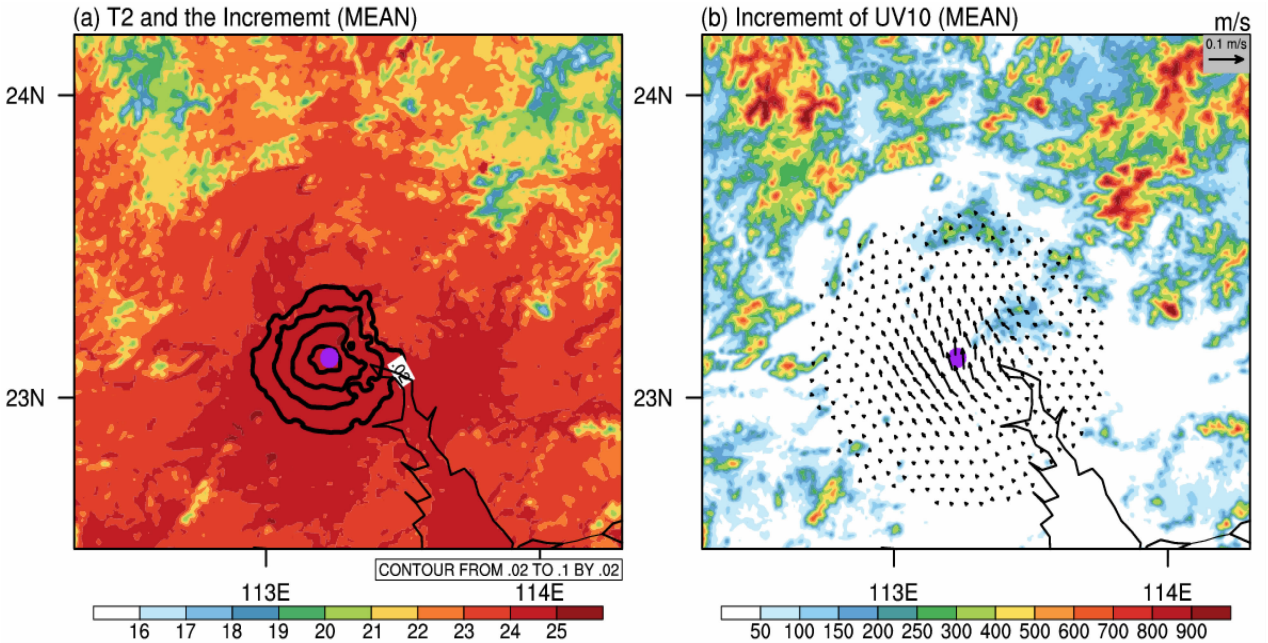

Figure 6. Horizontal distributions of 2-m temperature (shaded) and its increments (a) and the increments 10-m wind field (b, shaded for terrain height) after assimilating single point data (purple point) at 2300 BST.

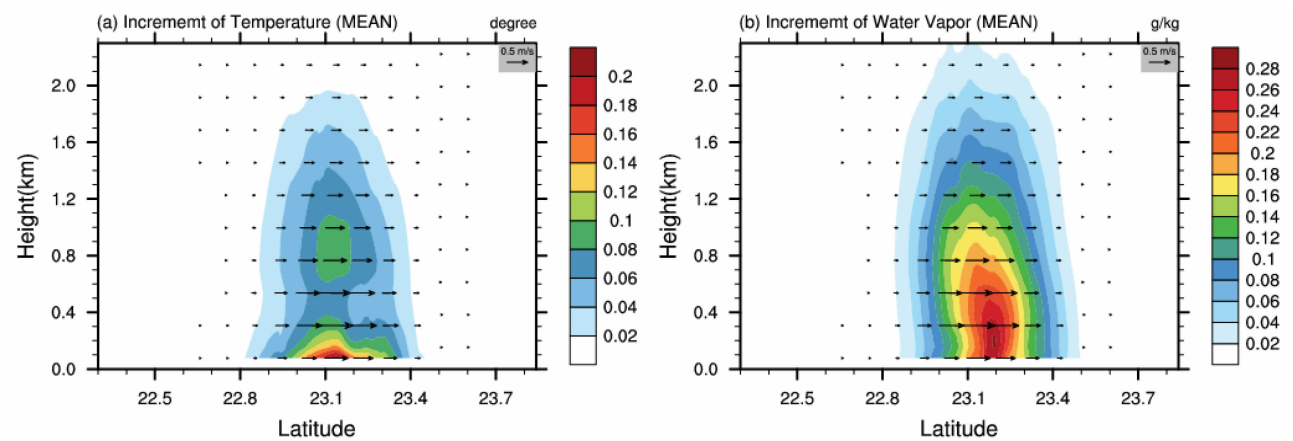

Figure 7. Vertical distributions of the increments of temperature (a), water vapor mixing ratio (b), and wind fields (vectors) along the station (longitude=113.231°E) after assimilating single point data at 2300 BST.

5 RESULTS AND ANALYSIS

5.1 *Analysis of the increments near-surface layer*

Figure 8 shows the differences of 10-m wind field, 2-m temperature, and 2-m water vapor mixing ratio before and after assimilation (observation data: 10-m wind, 2-m temperature, and 2-m mixing ratio of water vapor) at 2300 BST. After assimilation, the southerly wind over Guangzhou city and its southern area (south of 23.5°N) is increased, and there is a convergence of wind produced over the northern Guangzhou (near 23.5°N) and then it is enhanced within observation data. In experiment "NoDA" (without data assimilation), the simulated 2-m temperature is far below the meteorological observation data (color solid points in Fig. 8d), and the simulated 2-m water vapor mixing ratio is also lower. After assimilating observation data, the 2-m temperature and 2-m water vapor mixing ratio over the Pearl River Delta region are obviously increased, indicating that there are the increases in the near-surface temperature and moisture content. Additionally, the differences of them between observation and experiment "WithDA" are decreased compared with experiment "NoDA". The maximum change of increment is mainly distributed to the south of 23.3° N, while the extreme rainfall occurs downstream the maximum change (the north of the Pearl River Delta region, 23.2–23.5°N). Corresponding to the area of greatest change in temperature after assimilation is the urban area of Guangzhou. In summary, compared with experiment "NoDA", the results of experiment "WithDA" better reflect the state of the simulated region, especially the characteristics of dynamics and thermodynamics over the city region.

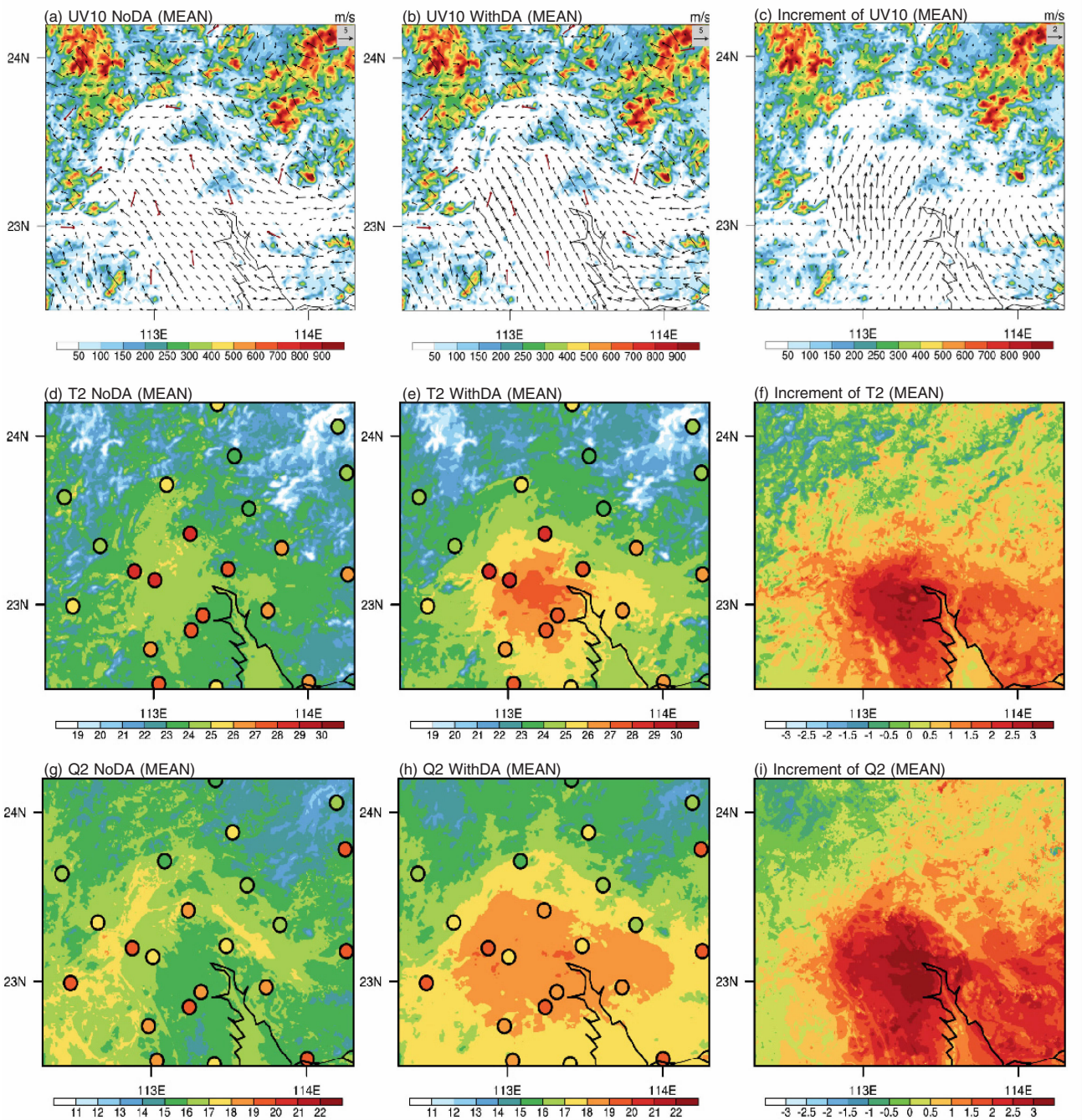

Figure 8. Ensemble mean fields of 10-m wind (m/s; a, b, c; color shaded: terrain height; red wind barb for observation), 2-m temperature (℃; d, e, f), and 2-m water vapor mixing ratio (g/kg; g, h, i) for "NoDA" (first column), "WithDA" (second column), and increments (third column) at 2300 BST (observation data represented by color dots).

In order to understand better, the vertical distributions of temperature, wind, and pseudoequivalent potential temperature along the longitude of 113.22° E (near the center of city) are shown in Fig. 9. The temperature in both of experiments decrease with height below the height of 2 km. Without assimilation, the surface temperature is not greatly changed along the latitude (urban area). In experiment "WithDA", near-surface air temperature is significantly increased by about 3–5℃ with a maximum up to 29℃. Moreover, there is obvious change of surface temperature along the latitude. The impact of assimilating surface observation data is mainly concentrated in the height below 2 km, especially the height lower than 500 m (Fig. 9c). In addition, the maximum pseudoequivalent potential temperature below the height of 2 km is increased from 327 to 337 K after assimilation. In the surface layer, the pseudoequivalent potential temperature is increased with height in experiment "NoDA", while it is decreased with the rise of elevation in experiment "WithDA". The

temperature and water vapor are increased near the surface and the southerly wind is also enhanced with assimilation. The distribution of pseudoequivalent potential temperature inclines toward the downstream areas under the influence of southerly wind. After assimilation, the changes of air temperature and pseudoequivalent potential temperature are mainly distributed at the south of 23.5°N, where provides a warm and wet weather condition for extreme rainfall occurrence. The southerly wind is enhanced, and it takes more humid and warmer air from sea to land. Additionally, the urban heat island effect also leads to higher temperature near city. Moreover, due to topographic countercheck, there is a convergence of wind at 23.5°N and it is enhanced after assimilation, promoting the occurrence of convection and the vertical movement of air flow.

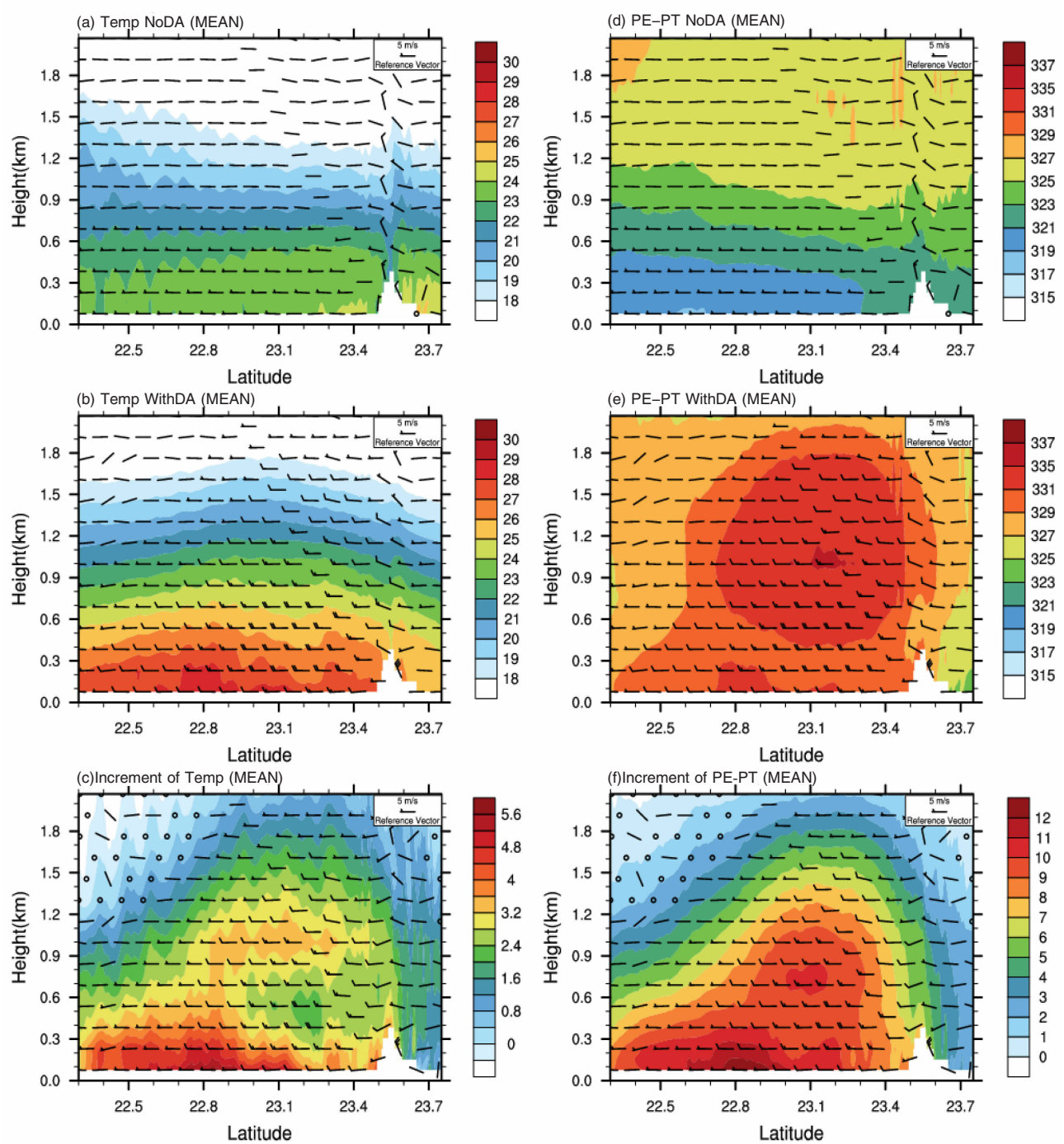

Figure 9. Vertical distributions of air temperature (℃; a, b), pseudoequivalent potential temperature (K; d, e) and the increments of them (c, f) along the longitude of 113.22°E at 2300 BST (first line for "NoDA"; second line for "WithDA"; third line for increments).

5.2 *Prediction of rainfall*

Figure 10 shows precipitation forecast within 12 hours from 2300 BST 6 May. In experiment "NoDA", the region of forecasting rainfall is to the north and the precipitation intensity is small compared to observation data. Moreover, there is no obvious rainfall in Guangzhou city (especially in the region to the south of 23.5° N). Assimilated observation data show that the predicted rainfall is almost distributed in Guangzhou city and its adjacent regions. The simulated rainfall intensity and distribution match with the observation well, that is, there is an obvious improvement in this extreme rainfall simulation by assimilating data. From observation data, rainfall starts in the hill of north Guangzhou city, and the 3-h calculated rainfalls (from 2300 to 0200 BST) exceeds 100 mm. However, the results from 60 ensemble members without assimilation deviate largely from the observed data (not shown), especially the intensity and pattern of rainfall. Moreover, there is almost no rainfall in 1/4 ensemble members and the accumulated rainfalls of most ensemble members are lower than 50 mm. Although the intensity and region of rainfall in the ensemble members with assimilation are different from observation, most of ensemble members can show the heavy rainfall in or around Guangzhou city.

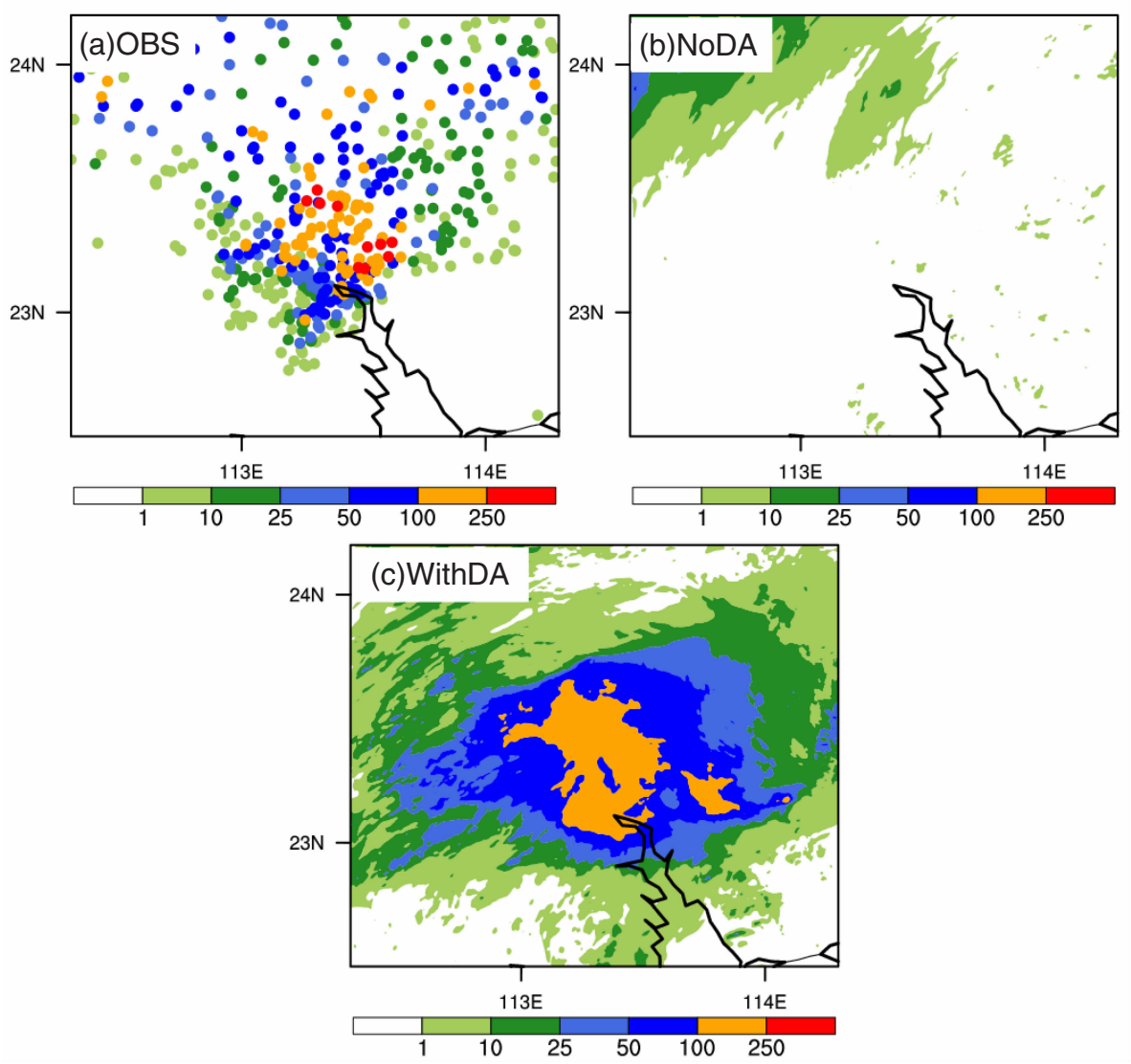

Figure 10. 12-h accumulated precipitation (mm) from 2300 BST 6 May to 1100 BST 7 May: (a)observation data, (b)experiment "NoDA", and (c)experiment "WithDA".

5.3 *Analysis of the forecasted temperature and humidity*

In order to analyze the forecasted results, Fig. 11 shows the averaged 2-m temperature and 2-m relative humidity from the observed stations of domain 3. According to observed data, averaged temperature decreases gradually from 0000 to 0700 BST and then increases after 0800 BST. The changes of averaged temperature in both experiments are similar to observation. The difference of averaged temperature between experiment "WithDA" and observation data is

mostly smaller than 2 K, and it is also smaller than that between experiment "NoDA" and observation. Compared to the observation, the simulated temperature is lower before 0800 BST and the simulated relative humidity is higher. As shown in Fig. 8, the 2-m temperature in experiment "WithDA" is still lower than that in observation, but it is better than that without assimilation. Hence, the simulated 2-m temperature is lower at night.

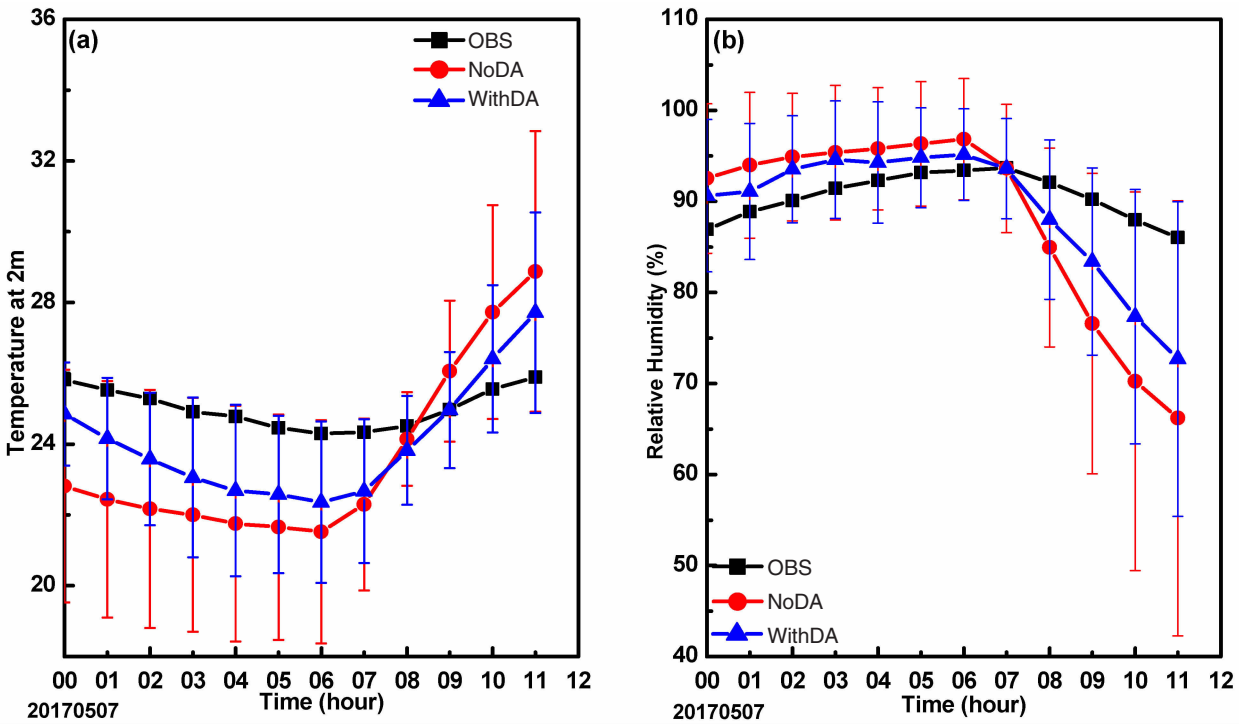

Figure 11. The evolution of averaged 2-m air temperature (℃; a) and 2-m relative humidity (%; b).

5.4 *Sensitivity tests of key factors*

As shown above, the assimilation of 10-m wind, 2-m temperature, 2-m vapor mixing ratio can improve the forecast of this severe rainstorm. In order to further study the effect of observation data on this case, the data of 10-m wind (experiment "DA_UV"), 2-m temperature (experiment "DA_TT"), and 2-m vapor mixing ratio (experiment "DA_QV") are assimilated, respectively, to investigate the significance of every observation data. The settings of these experiments are the same as above, and the deterministic forecast initiates from the ensemble mean of the EnKF system with assimilation at 2300 BST. Fig. 12 shows the prediction of 12-h precipitation from these three experiments. Experiment "DA_UV" and experiment "DA_QV" show similar characteristics of rainfall distribution and intensity, with main rainfall distribution lying on the north of 23.5°N. Compared to the observation, the intensity and location of these two experiments are weaker and more northerly. However, the amount and scope of rainfall increase slightly after assimilating 10-m wind and 2-m vapor mixing ratio (compared with experiment "NoDA"). In experiment "DA_TT", there is a rain belt with a 12-h accumulated precipitation greater than 100 mm, located at 23–23.5°N. The intensity and distribution of rainfall can successfully reproduce after assimilating 2-m temperature, but the rainfall intensity is weaker, and the main rainfall belt is to the east as compared with the observation.

Figure 13 shows the vertical distribution of pseudoequivalent potential temperature along the longitude of 113.22° E. Compared with experiment "NoDA", the pseudoequivalent potential temperature in the lower atmosphere increase slightly after assimilating 2-m temperature or 2-m vapor mixing ratio, but the pseudoequivalent potential temperature in experiment "DA_UV" and experiment "DA_QV" increase with height, which is similar to the experiment without assimilation (experiment "NoDA"). In experiment "DA_TT", the pseudoequivalent potential temperature in the lower atmosphere increases firstly and then decreases with the height, and it reaches the maximum (337 K) at about the height of 900 m. On the one hand, the increase in surface temperature can describe the urban heat effect correctly. On the other hand, the southerly wind is adjusted to take more warm air from the south to increase the surface temperature near city. As shown above, this rainstorm can be reproduced in experiment "WithDA" and experiment "DA_TT", implicating that assimilating 2-m temperature is the key factor in this case. This shows that the rainstorm may be related to the urban heat island effect.

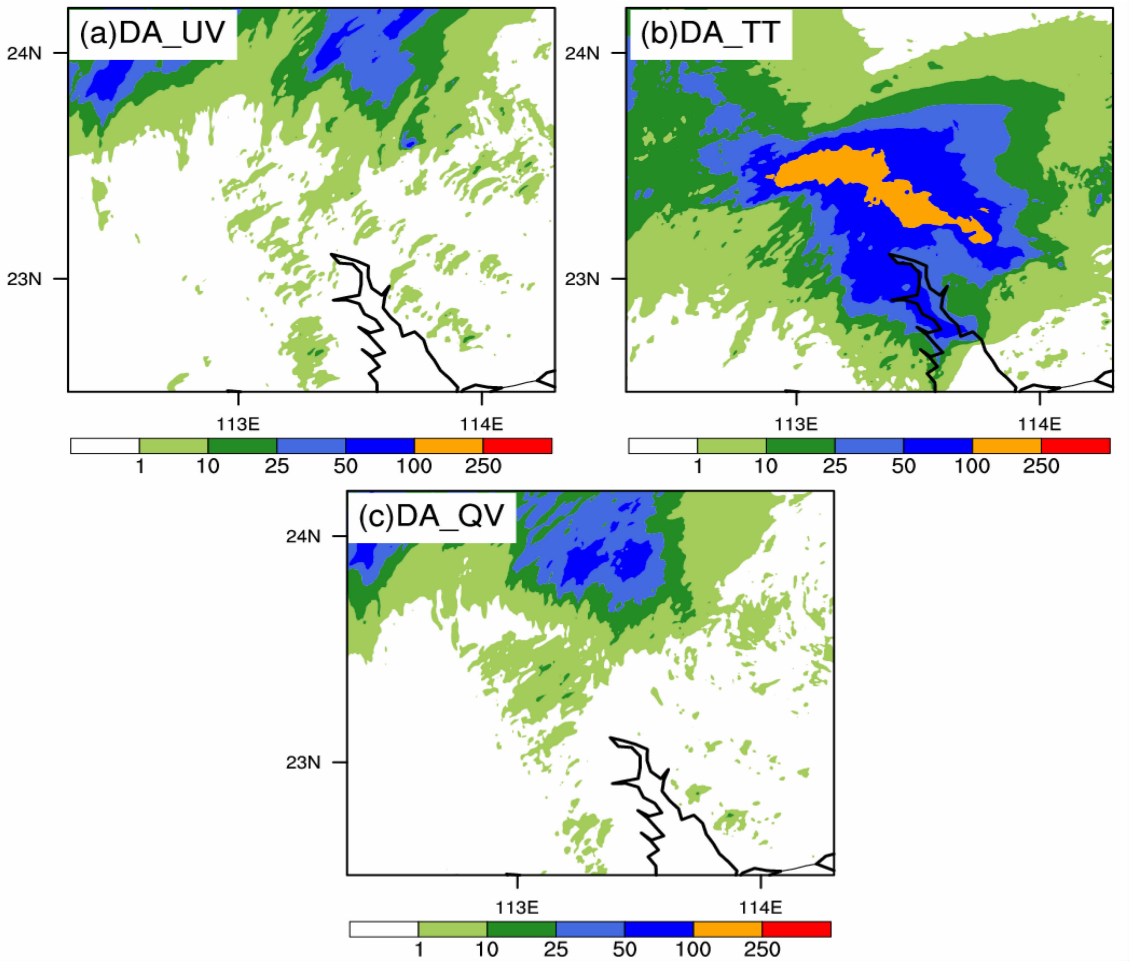

Figure 12. The prediction of 12-h accumulated precipitation (mm) from 2300 BST 6 May to 1100 BST 7 May: (a) experiment "DA_UV", (b) experiment "DA_TT", and (c)experiment "DA_QV".

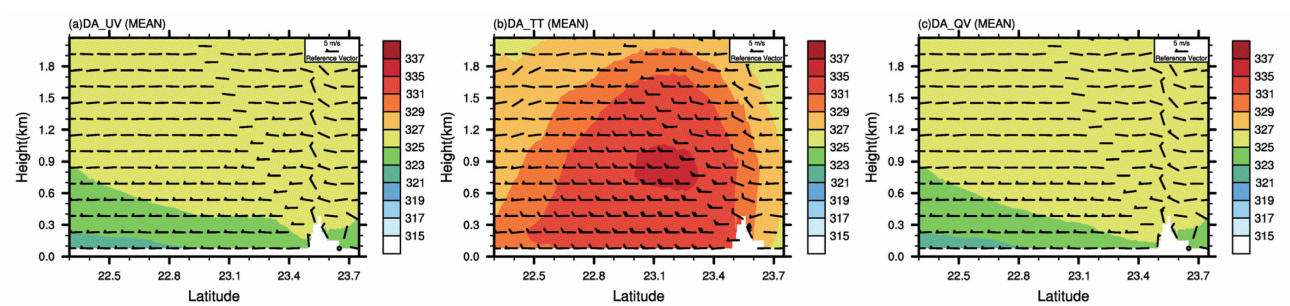

Figure 13. Vertical cross sections of pseudoequivalent potential temperature along the longitude of 113.22° E at 2300 BST: (a) experiment "DA_UV", (b) experiment "DA_TT", and (c)experiment "DA_QV".

6 SUMMARY

The Weather Research and Forecasting model with ensemble Kalman filter (WRF-EnKF) is used to assimilate the observation data of 10-m wind, 2-m temperature, and 2-m water vapor mixing ratio during a severe rainstorm in the Pearl River Delta region on 7 May 2017. Results show that the rainfall intensity and distribution in this case can be successfully reproduced by assimilating surface observation data.

After assimilating, the meteorological factors are significantly adjusted below the height of 2 km, such as wind field, temperature and water vapor. The southerly wind over Guangzhou city and the south of the Pearl River Delta region is enhanced, and the convergence of wind over the northern Guangzhou city is also enhanced. Moreover, the temperature, water vapor mixing ratio and pseudoequivalent potential temperature are obviously increased over the urban region, especially below the height of 2 km, providing a beneficial condition for the occurrence of extreme rainstorms. With data assimilation, the forecasts of rainfall amount, 2-m temperature and 2-m relative humidity are significantly improved, especially the intense precipitation area (12-h rainfall amount >100

mm). Meanwhile, the deviations of 2-m temperature and 2-m relative humidity decrease greatly over the simulated region. Additionally, the results of sensitivity tests indicate that the key to the prediction of this extreme rainfall event is the assimilation of 2-m temperature, and just assimilating data of surface wind or water vapor is not workable.

Overall, urban heat island effect may be an important factor in the prediction of this extreme rainstorm. Hence, accurate description of urban heat island effect plays a vital role in this case. In this study, WRF-EnKF has been used to better describe the urban heat island effect by assimilating observation data, thus improving the prediction ability on extreme rainfall over the city region. For now, the work is still preliminary, and it needs further systematic analysis to study how urban heat island effect influences the development of extreme rainstorms.

REFERENCES:

[1] ZHANG R, NI Y, LIU L, et al. South China Heavy Rainfall Experiments (SCHeREX)[J]. J Meteor Soc Jpn, 2011, 89A: 153-166.

[2] LUO Y, ZHANG R, WAN Q, et al. The Southern China Monsoon Rainfall Experiment (SCMREX)[J]. Bull Amer Meteor Soc, 2017, 98(5): 999-1013.

[3] ZHANG F, WENG Y, SIPPEL J A, et al. Cloud-resolving hurricane initialization and prediction through assimilation of Doppler radar observations with an Ensemble Kalman Filter[J]. Mon Wea Rev, 2009, 137(7): 2105-2125.

[4] WENG Y, ZHANG F. Assimilating airborne Doppler radar observations with an ensemble Kalman filter for convection-permitting hurricane initialization and prediction: Katrina (2005) [J]. Mon Wea Rev, 2012, 140 (3): 841-859.

[5] ZHU L, WAN Q, SHEN X, et al. Prediction and predictability of high-impact western Pacific landfalling tropical cyclone Vicente (2012) through convection-permitting ensemble assimilation of Doppler radar velocity[J]. Mon Wea Rev, 2016, 144(1): 21-43.

[6] BAO Xing-hua, LUO Ya-li, SUN Jia-xiang, et al. Assimilating Doppler radar observations with an ensemble Kalman filter for convection-permitting prediction of convective development in a heavy rainfall event during the pre-summer rainy season of south China[J]. Sci China: Earth Sci, 2017, 60(10): 1866-1885.

[7] ZHANG Cheng-zhong, CHEN Zi-tong, WAN Qi-lin, et al. Application experiment of assimilating radar-retrieved water vapor in short-range forecast of rainfall in the annually first rainy season over south China [J]. J Trop Meteor, 2016, 22(4): 578-588.

[8] WAN Q L, XU J J. A numerical study of the rainstorm characteristics of the June 2005 flash flood with WRF/GSI data assimilation system over south-east China [J]. Hydrological Processes, 2011, 25(8): 1327-1341.

[9] WAN Qi-lin, XU Jian-jun, HE Jin-hai. Impacts of ATOVS data assimilation on prediction of a rainstorm over southeast China[J]. J Trop Meteor, 2009, 15(2): 155-161.

[10] HACKER J P, SNYDER C. Ensemble Kalman filter assimilation of fixed screen-height observations in a parameterized PBL [J]. Mon Wea Rev, 2005, 133 (11): 3260-3275.

[11] ZHANG F, MENG Z, AKSOY A. Tests of an ensemble Kalman filter for mesoscale and regional-scale data assimilation, Part I: Perfect model experiments [J]. Mon Wea Rev, 2006, 134(2): 722-736.

[12] HUANG Yan-yan, XUE Ji-shan, WAN Qi-lin, et al. Improvement of the surface pressure operator in GRAPES and its application in precipitation forecasting in south China[J]. Adv Atmos Sci, 2013, 30(2): 354-366.

[13] OKE T R. The energetic basis of the urban heat island[J]. Quart J Roy Meteor Soc, 1982, 108(455): 1-24.

[14] MAGEE N, CURTIS J, WENDLER G. The urban heat island effect at Fairbanks, Alaska [J]. Theor Appl Climatol, 1999, 64(1): 39-47.

[15] HUFF F A, CHANGNON S A. Climatological assessment of urban effects on precipitation[J]. J Appl Meteor, 1972, 11(5): 823-842.

[16] EVENSEN G. Sequential data assimilation with a nonlinear quasi-geostrophic model using Monte Carlo methods to forecast error statistics [J]. J Geophys Res, 1994, 99(5): 10143.

[17] HOUTEKAMER P L, HERSCHEL L M, GERARD P, et al. Atmospheric data assimilation with an Ensemble Kalman Filter: Results with real observation[J]. Mon Wea Rev, 2005, 133(3): 604-620.

[18] ZHANG F, ZHANG M, POTERJOY J. E3DVar: Coupling an Ensemble Kalman Filter with three-dimensional variational data assimilation in a limited-are weather prediction model and comparison to E4DVAar[J]. Mon Wea Rev, 2013, 141(3): 900-917.

[19] MENG Z, ZHANG F. Test of an ensemble Kalman filter for mesoscale and regional-scale data assimilation, Part III: Comparison with 3DVAR in a real-data case study[J]. Mon Wea Rev, 2008a, 136(2): 522-540.

[20] MENG Z, ZHANG F. Test of an ensemble Kalman filter for mesoscale and regional-scale data assimilation, Part IV: Performance over a warm season month of June 2003[J]. Mon Wea Rev, 2008b, 136(10): 3671-3682.

[21] MORRISON H, PINTO J O. Mesoscale modeling of spring time Arctic mixed-phase stratiform clouds using a new two-moment bulk microphysics scheme [J]. J Atmos Sci, 2005, 62(10): 3683-3704.

[22] NOH Y, CHEON W G, HONG S Y, et al. Improvement of the K-profile model for the planetary boundary layer based on large eddy simulation data [J]. Bound-Layer Meteor, 2003, 107(2): 401-427.

[23] GRELL G A, FREITAS S R. A scale and aerosol aware stochastic convective parameterization for weather and air quality modeling [J]. Atmos Chem Phys, 2014, 13(9): 5233-5250.

[24] LI Ji-hang, WAN Qi-lin, GAO Yu-dong, et al. The effect of sample optimization on the ensemble Kalman filter in forecasting Typhoon Rammasun (2014) [J]. J Trop Meteor, 2018, 24(4): 433-447.

Citation: XIAO Hui, WAN Qi-lin, LIU Xian-tong, et al. Numerical prediction of an extreme rainstorm over the Pearl River Delta region on 7 May 2017 based on WRF-EnKF[J]. J Trop Meteor, 2019, 25(3): 312-323.